Measuring absolute infrared spectral radiance with correlated photons: new arrangements for improved uncertainty and extended IR range

E. Dauler, A. Migdall, N. Boeuf, R. U. Datla, A. Muller and A. Sergienko

Abstract. New experimental configurations of a system to measure absolute infrared (IR) spectral radiance using correlated photons are presented. The method has the remarkable feature that it allows spectral radiance to be measured in the IR in an intrinsically absolute manner, using only uncalibrated, visible detectors. Previous tests of this method have demonstrated its feasibility by making radiance measurements at wavelengths as long as 5 μm with relative standard uncertainties of less than 2 %. A new configuration of the previously tested $LiIO_3$ down-conversion crystal is proposed that allows measurements with better efficiencies and lower uncertainties. A second proposal to measure radiance at 8 μm using a new IR crystal is also discussed.

1. Introduction

Previous work has demonstrated that spectral radiance can be measured using correlated photons [1-4]. That work outlined some of the useful features of the method. One such feature is that it measures spectral radiance in an intrinsically absolute manner that does not need externally calibrated standards [5, 6]. In addition, the method allows radiance to be measured in the IR using only visible-wavelength (VIS) detectors and visible-wavelength selective elements, the latter to set the bandwidth of the IR radiance measurements. The use of VIS detectors with their intrinsically superior characteristics, instead of IR detectors, is another major advantage of the method. In fact, the method does not even require the VIS detectors to be calibrated: in general, the only constraint on them is good linearity. Here we propose two new measurement arrangements that can lead to improved uncertainty and greater IR spectral coverage. One arrangement uses a new configuration of the down-conversion crystal used in the previous measurements to achieve better uncertainty; the second arrangement uses a new type of crystal that allows radiance to be measured out to at least 8 μm. As a basis for understanding the improvements proposed in this paper, the principle of the measurement method and a brief review of the previous tests are given first.

E. Dauler, A. Migdall, N. Boeuf and R. Datla: Optical Technology Division, 221/B208, National Institute of Standards and Technology, Gaithersburg, MD 20899, USA.
A. Muller and A. Sergienko: Department of Electrical and Computer Engineering, Boston University, 44 Cummington St., Boston, MA 02215, USA.

2. Correlated photon method

The correlated photon method measures spectral radiance [4, 5] using the process of optical parametric down-conversion in which photons from a pump beam, in effect, "decay" within a nonlinear medium into pairs of photons (arbitrarily referred to as signal and idler photons). These photon pairs are created subject to the constraints of energy and momentum conservation (or phase matching):

$$\omega_{\mathrm{pump}} = \omega_{\mathrm{idler}} + \omega_{\mathrm{signal}}, \tag{1}$$

$$\vec{k}_{\mathrm{pump}} = \vec{k}_{\mathrm{idler}} + \vec{k}_{\mathrm{signal}}, \tag{2}$$

where ω and $\vec{k}$ are, respectively, the frequency and momentum of the photon indicated by its subscript [7]. Because these photons are created two at a time and because of these constraints, the measurement of one photon's direction and energy can be used to determine the direction and energy of the correlated photon. (In the application discussed here, where radiance well into the IR is measured with a VIS detector, highly spectrally non-degenerate IR-VIS photon pairs are used.) By adding infrared radiation to the nonlinear crystal, so as to overlap with the IR output in direction and spectrum, the down-conversion process can be enhanced or "stimulated", increasing the production of IR photons, but because the photons must be created in pairs, the VIS channel is also stimulated. In this

way, a VIS sensor can be used to "see" the IR radiation. The absolute radiance is determined by the ratio of the visible signal, stimulated by the IR beam, to the "unstimulated" visible signal. This is because the unstimulated down-converted output can itself be thought of as being stimulated by a background radiance of 1 photon/mode [6, 8]. The radiance of the unknown source, in units of photon/mode, is then just this ratio (excluding IR coupling terms discussed below). This 1 photon/mode radiance can be written in terms of fundamental constants as hc^2/λ^5 to obtain radiance in the more conventional units of W/(m^3 sr). The derivation of this is explained in more detail in [4].

3. Basic experimental setup and proposed improvements

Figure 1a shows the general scheme to measure radiance using correlated photons. The incident pump beam, $\lambda_{\rm pump}$, and the down-converted photon pair, $\lambda_{\rm VIS}$ and $\lambda_{\rm IR}$ created within the crystal of length L, are shown. Their output angles, $\theta_{\rm VIS}$ and $\theta_{\rm IR}$, are determined by (1) and (2) (used in conjunction with the crystal indexes and the orientation of the crystal optic axis). The IR radiance to be measured is produced by an Ar arc source [9], which is shown aligned to overlap with the down-converted IR output beam. An anti-reflection-coated Si filter, which blocks visible light from the IR source, is used to ensure that only down-converted light is measured by the VIS detector. A ZnSe lens is used to image the IR source into the crystal. A shutter in the IR beam path allows the down-conversion to be switched between spontaneous and stimulated modes. A narrow bandpass filter is placed in front of the VIS detector to limit the detected spectrum. The detector iris may also limit the spectrum seen by the detector as described below. The detector lens is used to concentrate all the light passing through the iris on to the detector. Table 1 gives the angles of the IR and visible beams for the original and new configurations at the two IR wavelengths measured, as well as the centre wavelengths and bandpasses of the visible filters used. The new, smaller $\theta_{\rm IR}$ angles were obtained by orienting the crystal optic-axis at 26.1° from the pump direction. (The crystal was cut with its optic axis oriented at 34° to the crystal surface normal.) In addition to the changes noted in the table, the new configuration uses a thinner crystal (3 mm versus approximately 10 mm) with its optic axis rotated 18° about the pump axis direction.

The proposed improvements in uncertainty expected with the new configuration are best illustrated by direct comparison with the original setup. Table 2 shows the net effects on uncertainty of using the new angles shown in Table 1, for the two IR wavelengths (3.415 μm and 4.772 μm), where the original tests of the method were made. The conventional measurements of the previous work [4] are given to allow comparison of the uncertainties between the methods. A discussion of the individual components of both tables is given in the following sections.

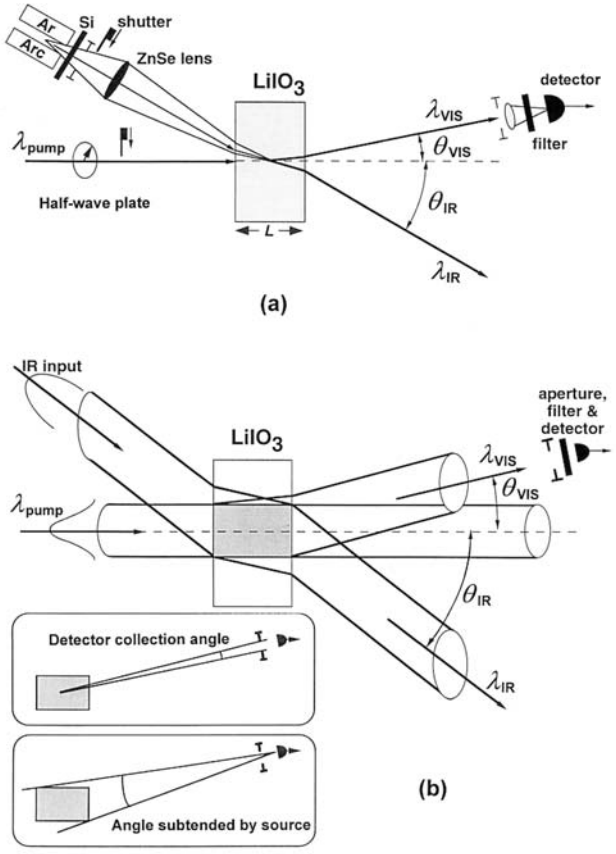

Figure 1. (a) Scheme for absolute radiance measurement using parametric down-conversion. (b) Diagram of pump and IR beam interaction region size as viewed from above.

Table 1. Bandpass for uncertainty improvement experiment. All angles are external to the crystal.

$\lambda_{\rm IR}$/μm	$\theta_{\rm IR}$/°	$\lambda_{\rm VIS}$/nm	$\Delta\lambda_{\rm VIS}$/nm (filter) FWHM	$(\Delta\theta_{\rm VIS}/\Delta\lambda_{\rm VIS})$/ (mrad/nm)	$\Delta\theta_{\rm VIS}$/ mrad	$\Delta\lambda_{\rm VIS}$/nm (geom) FWHM	$\Delta\lambda_{\rm IR}$/nm FWHM	$(\Delta\theta_{\rm IR}/\Delta\lambda_{\rm IR})$/ (mrad/nm)	$\Delta\theta_{\rm IR}$/ mrad FWHM	Configur-ation
3.415	24.62	528.8	6.0	–0.542	1.89	3.478	145.0	0.247	35.8	Original
	14.1			1.360	1.84	1.354	58.0	0.307	17.3	New
4.772	44.86	506.5	3.0	0.319	1.90	5.946	267.0	0.186	49.6	Original
	32.3			0.131	1.86	14.215	267.0	0.158	42.2	New

Table 2. Comparison of efficiencies and uncertainties for new and old experimental configurations at two IR wavelengths λ. $N_{\rm stim}$ and $N_{\rm spont}$ are the numbers of stimulated and spontaneous photons. Radiances $L_{\rm corr}$ and $L_{\rm conv}$, respectively, are the values obtained by the new correlated method (ratio/efficiency) and by the conventional method with a bandpass filter. The dashes indicate unchanged values; predicted values are indicated by an asterisk. The relative standard uncertainties are given in parentheses.

	$\lambda = 3.415$ μm		$\lambda = 4.772$ μm	
	Old	New	Old	New
IR beam transmittance				
Si filter transmittance	0.9392(0.0053)	–	0.8444(0.0059)	–
ZnSe lens transmittance	0.9250(0.0054)	–	0.9589(0.052)	–
$LiIO_3$ half crystal transmittance	0.9044(0.0031)	0.9093(0.0009)	0.8503(0.0089)	0.9136(0.0008)
one-surface reflectance	0.0814(0.0002)	0.0841(0.0003)	0.0968(0.0029)	0.0695(0.0006)
internal transmittance	0.9846(0.0031)	0.9928(0.0009)	0.9414(0.0084)	0.9819(0.0005)
Total IR signal transmittance	0.7857(0.0082)	0.7900(0.0076)	0.6885(0.0119)	0.7397(0.0079)
Total overlap factor	0.9376(0.0041)	0.9921(0.0002)	0.8220(0.0134)	0.9464(0.0011)
spatial overlap factor	0.9460	0.9950	0.8576	0.9726
angular overlap factor	0.9911	0.9971	0.9585	0.9731
Total system efficiency	0.7367(0.0091)	0.7838(.0076)	0.5659(0.0179)	0.7001(0.0080)
Ratio $N_{\rm stim}/N_{\rm spont}$	0.4381(0.0072)	0.475*	0.9380(0.0051)	1.189*
$L_{\rm corr}$/(photon/mode)	0.5947(0.0117)	(0.0105)	1.6575(0.0186)	(0.0095)
$L_{\rm conv}$/(photon/mode)	0.6057(0.0130)		1.6455(0.0322)	
$(L_{\rm conv}-L_{\rm corr})/L_{\rm conv}$	0.018(0.018)		–0.007(0.037)	

3.1 Uncertainty improvement

3.1.1 System efficiency

In extracting a spectral radiance of the IR source using this method, it is useful to define a system efficiency as was done in [4]. This quantity is used to determine the radiance at the IR source rather than just the radiance within the crystal. It takes account of all IR losses in coupling the source radiance into the crystal, where it can stimulate the down-conversion process. A second component of the efficiency depends on how well the IR beam overlaps (spatially and angularly) the region of the crystal pumped by the laser (see Figure 1b). The first goal of this work, uncertainty improvement, is accomplished generally by reducing the IR losses and increasing the IR-pump beam overlap, thus reducing the uncertainties associated with estimating the efficiency factor. IR losses can be reduced by the proposed configuration in two ways: (i) IR reflective loss at the crystal input surface is reduced by decreasing the incident angle of the IR input beam and by using an arrangement where Brewster's angle is approximated; and (ii) IR absorptive loss is reduced by decreasing the crystal thickness. Fortunately, these two modifications to reduce IR losses also improve the IR-pump beam overlap factor, because both reduce the transverse extent of the pumped region as viewed along the IR beam path (see the lower inset of Figure 1b). Reducing the angle between the pump and IR beam improves the overlap through an additional mechanism: the smaller angles reduce the angular spread of the IR beam correlated with the visible beam detected, thus reducing the angular extent of the region that must be filled by the beam to be measured.

As seen in Table 2, the biggest change of IR beam transmittance was the reduction in the crystal reflectance at 4.772 μm, with a decrease of $\sim$30 %. This was achieved by rotating the crystal 51° about the pump direction to obtain an incident angle near Brewster's angle with proper polarization orientation. For the measurement at 3.415 μm, the reflectance is actually slightly larger owing to a larger crystal tilt used to reduce $\theta_{\rm IR}$ which improved the overlap. The internal transmittance was increased as a result of the reduction in the thickness of the crystal. These changes combine to improve the total IR signal transmittance slightly at 3.415 μm and by about 10 % at 4.772 μm along with a reduction in uncertainty of over 30 % at that wavelength. (Of course, the IR transmittances of the Si filter and the ZnSe lens were unchanged by the changes in the crystal orientation.)

The overlap factor, which describes how well the IR beam overlaps the region of the crystal pumped by the laser, consists of two components: a spatial overlap and an angular overlap. The spatial overlap is obtained by calculation from the pump beam and IR beam profiles and directions. The pump beam is assumed to be Gaussian in profile (its diameter was measured at the position of the crystal). The measured profile of the IR beam was fitted to a parabolic form with a zero-level cutoff. This shape is scaled by the magnification of the imaging system. These two profiles (at the incident angles of the setup) were then convolved within the crystal to obtain the spatial overlap factor.

The angular overlap factor is determined by how well the angular extent of the IR beam fills the angular region that contributes to the production of visible light detected by the VIS detector. To find the extent of this

angular region it is necessary to see how the spectral bandpass of the measurement is related to the angular geometry of the system.

3.1.2 Infrared measurement bandpass

Once the bandwidth of the detected visible radiation is determined, the bandwidth of the IR radiance measurement is found using (1). This VIS band may be limited by the spectral filter $\Delta\lambda_{\mathrm{VIS}}$ (filter) in front of the VIS detector or by the range of angles seen by that detector, $\Delta\theta_{\mathrm{VIS}}$ (geom). The angular geometry limits the measurement spectrum via the angular dispersion of the down-converted light versus angle. The range of angles seen by the detector may be limited by the detector collection angle or the angle subtended by the source as shown in the insets of Figure 1b. Table 1 summarizes the terms involved in determining the IR measurement bandwidth. The angular dispersion is used along with the range of angles seen by the detector to obtain $\Delta\lambda_{\mathrm{VIS}}$ (geom), the bandpass determined by geometric limitations. The final visible limit is determined from the smaller of the geometric or filter limits. This final limit then determines the IR bandwidth.

Table 1 shows that while the range of angles seen by the detector is nearly constant for all the measurements, the final IR bandwidths, $\Delta\theta_{\mathrm{IR}}$, vary significantly. This is due to the differing wavelength dispersions versus angle. It may be seen that for the 3.415 μm measurement, both the old and new configurations are limited by $\Delta\lambda_{\mathrm{VIS}}$ (geom), although the new configuration has a limit that is less than half the limit in the original setup. For the 4.772 μm measurement, both configurations are limited by $\Delta\lambda_{\mathrm{VIS}}$ (filter), so the correlated IR bandwidth is unchanged. The angular spread of the IR, $\Delta\theta_{\mathrm{IR}}$, is determined from the IR wavelength-versus-angle dispersion and the IR bandwidth. In both cases, the IR bandwidth is reduced in the new configuration, which makes it easier to achieve a high angular overlap factor.

The angular extent of the IR beam incident on the crystal is limited by the aperture (f number) of the imaging optics, which also determines the IR magnification. The angular overlap is calculated by convoluting the angular extent of the IR input beam with angular emittance of the down-converted IR beam, defined by the IR bandpass. The angular profile of the IR input beam is assumed to be constant with a sharp cutoff set by the clear aperture of the imaging lens. The angular intensity profile (of the IR down-converted light) used is Gaussian, with a full-width-half-maximum (FWHM) $\Delta\theta_{\mathrm{IR}}$, as shown in Table 1.

The overlap factors are affected by the IR imaging optics. By changing the magnification, the size of the beam and its angular extent can be varied, along with the overlap factors. The magnification must be optimized, because improving the spatial overlap by increasing the beam size at the crystal decreases the angular overlap as the angular extent of the IR beam is reduced. Magnifications of 4.39 and 1.98, respectively, were chosen for the new 3.415 μm and 4.772 μm measurements, to maximize the product of the angular and spatial overlap factors. The result of this magnification optimization, along with the improvements due to the thinner crystal, smaller angles, and smaller angular spreads, is shown in Table 2, where overlap factors at both measurement wavelengths much more closely approach 100 %, with their associated uncertainties now becoming essentially negligible. (Note that in the results previously reported in [4], the angular overlap had been assumed to be unity and was neglected. The inclusion of this factor here, as shown in Table 2, has significantly improved the final agreement of the original comparison of the two methods.)

In combining the new IR transmittances and the overlap factors, we find that the overall improvement in the system efficiency is about 6 % at the shorter wavelength, but nearly 25 % at the longer wavelength. The improvements in uncertainty exceed these values, with the 4.772 μm uncertainty reduction exceeding 50 %. The expected uncertainties of the new radiance measurements, as given in Table 2, are the quadrature sum of the efficiency uncertainty and the measured stimulated/spontaneous ratio (which for purposes of this comparison is assumed to be unchanged). To test these improved uncertainties independently, as was done in the original comparison, the conventional measurement uncertainties must also be reduced. Without such a reduction, the uncertainties of a new comparison would be dominated by the uncertainties in the conventional measurements of radiance, which now dwarf the new correlated radiance measurement uncertainties.

3.2 Infrared range improvement

The second improvement proposed in the current work is the extension to measurements beyond 5 μm. Although radiance can be measured using conventional methods far into the IR, the uncertainty increases as a result of decreasingly reliable detectors and the lack of calibrated standards. Since the correlated photon method allows IR radiance to be measured with visible detectors and without calibrated standards, it offers the possibility of accurate radiance measurements far into the IR. To extend the range of these measurements further into the IR, a number of requirements must be considered, including crystal transmittance, reflectance, phase matching and geometric factors related to bandwidth and overlap factors. These factors are discussed with respect to a proposed new system to allow measurements to 8 μm.

3.2.1 Crystal transmittance

For a particular crystal, the spectral range will be limited by its infrared transmittance. For the $LiIO_3$ of the previous experiments, this occurs at $\approx$5.5 μm, so a crystal with a longer transmission range is needed to measure radiance further into the IR. Most crystals that transmit beyond 6 μm have indices of refraction greater than 2. This usually leads to high reflectance that limits the system efficiency of experiments. To allow the radiance measurements to be made with high-quality VIS detectors requires one of the photons of a pair to be in the visible band. This means that in addition to passing the IR wavelength of interest and the correlated VIS photon, the crystal must also pass the even shorter wavelength VIS pump. After a search of crystal properties, GaSe was chosen for an experiment further into the IR. GaSe has a transmission range of 0.65 μm to 18 μm, although it has indices of refraction greater than 2.5 [10, 11]. As a first test of this crystal, we propose a radiance measurement at 8 μm. This wavelength was chosen as being significantly further into the IR than the previous $LiIO_3$ measurements, while maintaining manageable down-conversion angles. It should not be considered the limit for this crystal, which transmits to 18 μm.

3.2.2 Reflectance

A light beam at 8 μm, normal to the GaSe crystal, would have $\sim$22 % reflectance, greatly limiting the efficiency of a radiance measurement made using this crystal. However, most of this reflectance can be eliminated by sending the light in near Brewster's angle. For convenience, it would be best if both the pump and the IR beam can be sent in at Brewster's angle, to minimize the reflectance losses of both beams. Using a GaSe crystal with the optic axis normal to the surface (the usual way this crystal is available), a 0.85 μm pump must be sent in at 70.8° from the crystal normal to achieve minimum reflectance of the pump. Infrared at 8 μm will then be produced in a cone around the pump at an angle of 17.3° internal to the crystal and 56.4° external to the crystal. The output light will be polarized parallel to the plane of incidence for Brewster's angle reflectance and be perpendicular to the optic axis because it is an ordinary ray. Rotating the plane of incidence 25.4° allows Brewster's angle to be approximated, yielding a reflectance of only 0.69 %. This set-up allows both the pump and the IR source to be put in at angles near Brewster's angle and with the appropriate polarizations. This arrangement minimizes reflection to almost zero, but forces the detected visible light to come out at a large external angle ($\approx$76°).

3.2.3 Bandpass and overlap

A large external visible angle causes the angle subtended by the source to increase as the crystal is viewed more from the side. For a 3 mm thick GaSe crystal, the angle subtended by the source is $\sim$6 mrad (using the same detector-crystal distance as in the original $LiIO_3$ set-up). This leads to a large geometric bandpass that increases the angular spread that the infrared source must overfill. A relatively small IR beam magnification would help to fill this larger angular region; unfortunately this would also reduce the spatial overlap factor. Alternatively, the bandpass can be limited by a filter. A narrow filter reduces the detected angular spread and improves the angular overlap without affecting the spatial overlap. For a given filter bandpass, there is an optimum magnification that maximizes the product of the angular and spatial overlaps. Table 3 shows the results of bandpass calculations and optimum magnifications, along with their overlap factors, for three different bandwidth filters. From this, it may be seen that narrowing the bandpass of the filter greatly improves the overlap factor.

Limiting the bandpass using a narrow filter may also limit light reaching the detector to just a portion of the crystal. This could effectively further limit the thickness of the crystal and improve the overlap. However, the allowable angular deviation due to the momentum mismatch in a 3 mm thick crystal causes the detected light not to be limited to the centre of the crystal.

To evaluate the feasibility of using GaSe to measure radiance at 8 μm, a comparison with the $LiIO_3$ measurement is given in Table 4. The factors contributing to the system efficiency and expected signal are compared. For this calculation, we have assumed the same pump beam collimation as for the $LiIO_3$ setup, but because the pump is now much redder, the beam radius must be larger. (We have also assumed the same Si filter and ZnSe lens transmittances, as these are inherently irrelevant to this comparison.) This, along with the larger internal infrared angle, lowers

Table 3. Bandpass and corresponding detected angular spreads with different bandpass filters.

λ_{IR}/μm	θ_{IR}/°	λ_{VIS}/nm	$\Delta\lambda_{VIS}$/nm (geom) FWHM	$\Delta\theta_{VIS}$/ (mrad/nm)	$\Delta\lambda_{VIS}$/nm (filter) FWHM	Correlated $\Delta\lambda_{IR}$/nm FWHM	$(\Delta\theta_{IR}/\Delta\lambda_{IR})$/ (mrad/nm)	$\Delta\theta_{IR}$/mrad FWHM	Magni-fication	Total overlap factor
					10	709.0		170	1.4	0.422
8.0	56.4	951	16.7	0.11	3	212.0	0.234	51	2.0	0.855
					1	71.0		17	4.7	0.981

Table 4. Comparison of system configuration parameters for the previous $LiIO_3$ measurement at 4.77 μm and the proposed GaSe measurement at 8 μm. N_{stim}, N_{spont}, L_{corr} and L_{conv} are as defined in Table 2. The dashes indicate unchanged values; predicted values are indicated by an asterisk.

	$LiIO_3$ @$\lambda = 4.77$ μm	GaSe @$\lambda = 8$ μm
IR beam transmittance		
Si filter transmittance	0.8444	–
ZnSe lens transmittance	0.9589	–
$LiIO_3$ half crystal transmittance	0.8503	0.9931
one-surface reflectance	0.0968	0.0069
internal transmittance	0.9414	≈1
Total IR signal transmittance	0.6885	0.8041
Total overlap factor	0.8220	0.8548
spatial overlap factor	0.8576	0.9178
angular overlap factor	0.9585	0.9314
Total system efficiency	0.5659	0.6873
Ratio N_{stim}/N_{spont}	0.9380	≈3.44*
L_{corr}/(photon/mode)	1.6575	≈5*
L_{conv}/(photon/mode)	1.6455	≈5*

the overlap efficiency. However, a sufficiently narrow filter can be used to increase the infrared magnification, which would improve the total overlap efficiency. The figures listed in Table 4 are for the 3 nm bandpass filter, the same as was used in the $LiIO_3$ measurement.

This comparison shows that with GaSe, system efficiencies can be achieved that exceed those of the previous $LiI0_3$ measurement. In addition, the signal-to-noise ratio of this measurement should be quite high, as the radiance of the arc source at 8 μm is about three times the radiance at 4.77 μm. This should lead to uncertainties comparable with or lower than the $LiIO_3$ measurements.

4. Conclusion

We have shown that the correlated photon method of measuring IR spectral radiance can be expected to achieve relative standard uncertainties below 1% at 5 μm. This uncertainty is low enough that it may, in fact, be difficult to make a conventional measurement for direct comparison and verification purposes. We have also shown that the method can be extended to measure radiance to at least 8 μm, while maintaining the advantage of using convenient high-quality visible Si detectors. It should also be noted that the 8 μm measurement was chosen not because of the crystal transmittance limit, but because it was significantly beyond the 5 μm limit of the previous measurement and could be achieved without having angles that were too extreme. After gaining experience with this crystal in the proposed configuration, it is likely that measurements will be possible beyond 8 μm, as the crystal transmits up to 18 μm. These points highlight some of the potential advantages of this technique.

References

1. Kitaeva G. Kh., Penin A. N., Fadeev V. V., Yanait Yu. A., *Sov. Phys. Dokl.*, 1979, **24**, 564-566.
2. Penin A. N., Sergienko A. V., *Appl. Opt.*, 1991, **30**, 3582-3588.
3. Penin A. N., Kitaeva G. Kh., Sergienko A. V., *Proc. QELS'91 Balto.*, 1991, 110-112.
4. Migdall A., Datla R., Sergienko A., Orszak J. S., Shih Y. H., accepted by *Appl. Opt.*
5. Klyshko D. N., *Sov. J. Quantum. Electron.*, 1977, **7**, 591-594.
6. Klyshko D. N., *Photons and Nonlinear Optics*, New York, Gordon and Breach, 1988, 325 p.
7. Midwinter J. E., Warner J., *Br. J. Appl. Phys.*, 1965, **16**, 1135-1142.
8. Louisell W. H., Yariv A., Siegman A. E., *Phys. Rev.*, 1961, **124**, 1646-1654.
9. Bridges J. M., Migdall A. L., *Metrologia*, 1995/96, **32**, 625-628.
10. Nikogosyan D. N., *Sov. J. Quantum Electron.*, 1977, **7**, 1-13.
11. Abdullaev G. B., Kulevskii L. A., Prokhorov A. M., Savel'ev A. D., Salaev E. Yu., Smirnov V. V., *JETP Lett.*, 1972, **16**, 90-92.